# Efficient Computing of Far-Field Radiation in Two Dimension

Amedeo Capozzoli, *Member, IEEE*, Claudio Curcio, Angelo Liseno, and Jonas Piccinotti

***Abstract*—We deal with efficiently computing the far-field radiation/scattering by volumetric sources/objects. The approach consists of three steps: first, representation of "nonuniformly sampled" Fourier exponentials by a finite number of "uniformly sampled" ones, with such number controlling the accuracy; second, "pruned" fast Fourier transform; and third, interpolation, again with controlled accuracy, of the "uniformly sampled" exponentials onto the "nonuniformly sampled" ones corresponding to the relevant observation directions. The performance of the approach in terms of accuracy and complexity is evaluated.**

***Index Terms*—Computational electromagnetics, electromagnetic radiation, fast Fourier transforms (FFTs).**

## I. Introduction

THE computation of the far-field radiation/scattering by free-space sources/objects takes place in many areas of electromagnetics [1], [2], as the repeated calculation of the far field in iterative solution or design approaches. Solving this problem by a brute-force approach requires managing a complexity that may be unacceptable for large problems, especially for a three-dimensional (3-D) case [3].

The observation that the far field of planar (in 3-D) or linear (in 2-D) radiators/scatterers can be computed by a standard fast Fourier transform (FFT) has pushed the development of algorithms to reduce the computational complexity. For example, Boag and Letrou [3] seek to achieve the same complexity of the FFT, however without the explicit use of the FFT. As a result, this trend is obtained only when sacrificing accuracy.

In this letter, we face the problem of computing the far-field radiation/scattering by 2-D objects (infinitely long cylinders) in three steps [4], which are as follows:

1) representation of "nonuniformly sampled" Fourier exponentials by a finite number of "uniformly sampled" ones, with such number controlling the accuracy;
2) "pruned" FFT [5];
3) interpolation, again with controlled accuracy, of the "uniformly sampled" exponentials onto the "nonuniformly sampled" ones corresponding to the relevant observation directions.

Manuscript received February 21, 2017; revised April 7, 2017; accepted April 12, 2017. Date of publication June 9, 2017; date of current version July 24, 2017. *(Corresponding author: Amedeo Capozzoli.)*

The authors are with the Dipartimento di Ingegneria Elettrica e delle Tecnologie dell'Informazione, Universitá di Napoli Federico II, Naples 80125, Italy (e-mail: a.capozzoli@unina.it; clcurcio@unina.it; liseno@unina.it; jonas.piccinotti@gmail.com).

Color versions of one or more of the figures in this letter are available online at http://ieeexplore.ieee.org.

Digital Object Identifier 10.1109/LAWP.2017.2694998

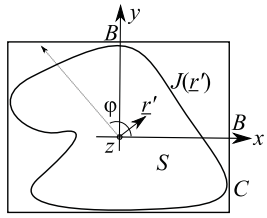


Fig. 1. Geometry of the infinitely long radiator/scatterer.

Since the output of the FFT step is needed at a few output points, and so the number of relevant output FFT points is less than the number of transform points, FFT "pruning" [5] enables the elimination of unrequired operations. As a consequence, the number of butterflies in the classical radix $2 \times 2$ FFT scheme or the number of operations within the butterflies may be reduced. Of course, similar pruning can be applied to eliminate operations on zeros when the number of input points is less than the number of transform points, but this will not be herein exploited. The role of the "pruned" FFT in mitigating the number of computations is also discussed.

## II. Far-Field Evaluation by Fourier Matrices

Let us consider a 2-D radiator/scatterer embedded in free space (see Fig. 1). The source $\underline{J}$ can be primary or can be the contrast source in the case of scattering [6]. Furthermore, and generally speaking, the support of $\underline{J}$ can be a curve, namely the boundary of $S$, or it can be formed by the points interior to $S$. Here, we assume that the support of $\underline{J}$ is $S$.

Without losses of generality, we consider a $z$-directed current $\underline{J} = J\hat{i}_z$. Then, the only ($z$) component of the far-field pattern (FFP) $P(\phi)$ (see Fig. 1), apart from unessential factors, is

$$P(\phi) = \int_S J(\underline{r}')e^{j\beta\underline{r}'\cdot\hat{i}_r}\,dS \tag{1}$$

where $\hat{i}_r = (\cos\phi, \sin\phi)$ and $\underline{r}' = (x', y')$.

Following the application of a quadrature rule [7], the FFP at the discrete angles $\phi_k$, $k = 1, \ldots, K$, can be written as

$$P(\phi_k) = F(s,t)|_{(s,t)=-(\beta\cos\phi_k, \beta\sin\phi_k)} = \sum_{i=0}^{N-1} w_i J_i e^{-j(x_i' s + y_i' t)}\Big|_{(s,t)=-(\beta\cos\phi_k, \beta\sin\phi_k)}. \tag{2}$$

We are then dealing with two grids: one in the spatial $(x, y)$ plane as defined by the $(x_i', y_i')$'s, and one in the spectral $(s, t)$ plane as defined by the $(s_k, t_k) = -(\beta\cos\phi_k, \beta\sin\phi_k)$'s.

Equation (2) can be recast as a matrix-vector multiplication $\underline{P} = \underline{\underline{A}}\ \underline{f}$, where $\underline{P}$ is the vector of the $P(\phi_k)$ s, $\underline{f}$ is the vector of the $w_i J_i$ s, and the elements of the $K \times N$ matrix $\underline{\underline{A}}$ are the $\exp\left[-j(x_i' s_k + y_i' t_k)\right]$'s. Matrix $\underline{\underline{A}}$ resembles, but is not in the form of, a Fourier matrix, namely a matrix $\underline{\underline{F}}_M$ whose generic $(ijpq)$th element is $\omega_M^{ijpq}$, $\omega_M$ being equal to $\exp[-j2\pi/M]$, namely a root of unity. The efficient computation of the FFP amounts thus at the efficient calculation of a matrix-vector multiplication, whose complexity strongly depends on the structure of the matrix. Fortunately, when $\underline{\underline{A}}$ has peculiar characteristics (e.g., Vandermonde matrix or Fourier matrix), the complexity can be significantly improved. Morgenstern's theorem [8] in the *c-restricted* computational model has been a cornerstone result in algebraic complexity theory [9], stating that the complexity associated with Fourier matrices arising from 1-D problems of size $L$ be not less than $(L/2)\log_c L$. Accordingly, in the case of a Fourier matrix $\underline{\underline{F}}_M$, the asymptotic complexity drops to $M^2 \log M$. Recasting the calculation in terms of a matrix-vector multiplication, involving a Fourier matrix, thus becomes convenient.

The problem with (2) is that $\underline{\underline{A}}$ is not a Fourier matrix, so that reformulating the problem by interpolating nonuniformly sampled exponentials by uniformly sampled ones is in order. This can be achieved by the Poisson formula [10]

$$e^{-j\xi x} = \sqrt{2\pi}\frac{\sum_{m\in Z}\mathcal{F}[\Phi(\xi)e^{-j\xi x};m]e^{jm\xi}}{\sum_{m\in\mathbb{Z}}\Phi(\xi+2m\pi)e^{-j2m\pi x}} \tag{3}$$

where $\Phi$ is an appropriate interpolation window and $\mathcal{F}$ denotes Fourier transformation. Accordingly, a computational scheme analogous to a nonuniform FFT procedure of Type-3 [4] can be set up. We illustrate the procedure by assuming $\Phi$ to be Gaussian. This choice is motivated by the availability of bounds concerning the maximum errors pertaining the "uniformly discretized" operator mapping functions in the $(x, y)$ domain onto functions in the $(s, t)$ domain [4].

### A. Step #1

The contributions from nonuniformly spaced input sampling points corresponding to $\exp\left[-j(s_k x_i + t_k y_i)\right]$ are "spread" by Gaussian windows $\exp[-x^2/(4\tau_x) - y^2/(4\tau_y)]$ with parameters $\tau_x$ and $\tau_y$, to a regular grid $(n\Delta x, m\Delta y)$. Step #1 thus gives the following equation:

$$f_\tau^{-\sigma}(n\Delta x, m\Delta y) = \frac{e^{[\sigma_x(n\Delta x)^2+\sigma_y(m\Delta y)^2]}}{\sqrt{4\sigma_x\sigma_y}}$$
$$\sum_{i=0}^{N-1} f_i e^{-\left[\frac{(n\Delta x - x_i)^2}{4\tau_x}+\frac{(m\Delta y - y_i)^2}{4\tau_y}\right]} \tag{4}$$

with $f_i = w_i J_i$ and where the presence of the exponential function $\exp[\sigma_x x^2 + \sigma_y y^2]$ is related to the precompensation of the Gaussian window used in Step #3. Due to the rapid decay of the exponential functions, $f_i$ significantly contributes to only few samples of $f_\tau^{-\sigma}(n\Delta x, m\Delta y)$. On defining $\mathrm{Int}[\alpha]$, the nearest integer to $\alpha$, by letting $\xi_i = \mathrm{Int}[x_i/\Delta x]$ and $\eta_i = \mathrm{Int}[y_i/\Delta y]$, $i = 0, \ldots, (N-1)$, denote the nearest regular grid points to $x_i/\Delta x$ and $y_i/\Delta y$, respectively, and assigning $n' = n - \xi_i$ and $m' = m - \eta_i$, the contributions of each $f_i$ to $f_\tau^{-\sigma}(n\Delta x, m\Delta y)$ can be ignored when $|n'| > m_{\mathrm{sp}}$ or $|m'| > m_{\mathrm{sp}}$, where $m_{\mathrm{sp}}$ is a parameter properly selected according to the required accuracy. In other words, the summation in (4) can be truncated to $(2m_{\mathrm{sp}}+1)\times(2m_{\mathrm{sp}}+1)$ terms.

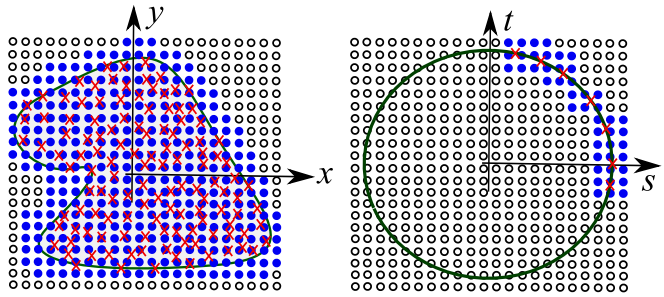


Fig. 2. Illustrating Step #1 (left) and Step #2 (right).

This step is illustrated in Fig. 2, where the current sample locations are red crosses, the black empty circles are the regular $(n\Delta x, m\Delta y)$ points, and the blue filled circles are the "spreading" due to (4) of the $(x_i', y_i')$ onto the $(n\Delta x, m\Delta y)$ grid.

### B. Step #2

The "spread" contributions are transformed to the spatial frequency domain via a standard FFT, thanks to the discretized version of the operator mapping the $(x, y)$ plane into the $(s, t)$ domain. In other words, the second step produces

$$F_\tau^{-\sigma}(p\Delta s, q\Delta t) \simeq \frac{\Delta x\Delta y}{2\pi}\sum_{n=-M_{r_x}/2m=-M_{r_y}/2}^{M_{r_x}/2-1}\sum^{M_{r_y}/2-1} f_\tau^{-\sigma}(n\Delta x, m\Delta y)$$
$$\times\, e^{-jpn\Delta x\Delta s}e^{-jqm\Delta y\Delta t}. \tag{5}$$

The FFT thus enables to evaluate $F(s, t)$ in (2) at the $(p\Delta s, q\Delta t)$'s, i.e., the black circles in Fig. 2 (right).

### C. Step #3

The "transformed" data are interpolated from the FFT output uniform grid to the nonuniform grid $\{(s_k, t_k)\}_{k=0}^{K-1}$, again by Gaussian windows, $\exp\left[-s^2/(4\sigma_x) - t^2/(4\sigma_y)\right]$. The final output is thus

$$P(\phi_k) = F(s_k, t_k) = \frac{\Delta s\Delta t}{4\pi\sqrt{\tau_x\tau_y}}e^{\tau_x s_k^2}e^{\tau_t t_k^2}$$
$$\sum_{n=-M_{r_x}/2}^{M_{r_x}/2-1}\sum_{m=-M_{r_y}/2}^{M_{r_y}/2-1} F_\tau^{-\sigma}(n\Delta s, m\Delta t)e^{-\frac{(n\Delta s - s_k)^2}{4\sigma_x}}e^{-\frac{(m\Delta t - t_k)^2}{4\sigma_y}}. \tag{6}$$

Similarly to Step #1, the presence of the Gaussian functions $\exp[\tau_x s^2 + \tau_y t^2]$ is related to the post-compensation of the Gaussian windows used in Step #1. Again due to the rapid decay of the involved exponential functions, $F_\tau^{-\sigma}(p\Delta s, q\Delta t)$ significantly contributes to only few samples of $F_\tau(s_k, t_k)$. In particular, on letting $\widetilde{\xi}_k = \mathrm{Int}[s_k/\Delta s]$, $k = 0, \ldots, (N_s - 1)$ and $\widetilde{\eta}_k = \mathrm{Int}[t_k/\Delta t]$, $k = 0, \ldots, (K-1)$, and $p' = p - \widetilde{\xi}_k$ and $q' = q - \widetilde{\eta}_k$, the contributions of $F_\tau^{-\sigma}(p\Delta s, \Delta t)$ can be ignored

TABLE I
SUMMARY OF THE PARAMETERS CHOICE

| $\Delta x = \frac{\pi}{\mathrm{RS}}$ | $\Delta y = \frac{\pi}{\mathrm{RT}}$ |
|---|---|
| $\Delta s = \frac{2\pi}{\Delta x M_{rx}}$ | $\Delta t = \frac{2\pi}{\Delta y M_{ry}}$ |
| $M_{rx} \geq 2\left(\frac{\mathrm{XSR}^2}{\pi} + 2\pi Rb\right)$ | $M_{ry} \geq 2\left(\frac{\mathrm{YTR}^2}{\pi} + 2\pi Rb\right)$ |
| $\tau_x = b\Delta x^2$ | $\tau_y = b\Delta y^2$ |
| $\sigma_x = b\Delta s^2$ | $\sigma_y = b\Delta t^2$ |

when $|p'| > m_{\mathrm{sp}}$ or $|q'| > m_{\mathrm{sp}}$. In other words, the summation in (6) can be truncated to $(2m_{\mathrm{sp}}+1) \times (2m_{\mathrm{sp}}+1)$ terms.

This step is illustrated in Fig. 2 (right), where the red crosses represent the sampling points at which the FFP is required, whereas the blue filled circles represent those regular grid points contributing to the value of the FFP samples of interest.

### D. "Centering" and Choice of the Relevant Parameters

Before applying the above-mentioned procedure, a "centering" of the input and output sampling points is required [4]. Similarly, for the choices of $\Delta x$, $\Delta y$, $\tau_x$, $\tau_y$, $\sigma_x$, $\sigma_y$, and $m_{\mathrm{sp}}$, see [4] and Table I. In such a table, $R$ is chosen strictly larger than 2, $X = \max\{|x'_i|\}_{i=0}^{N-1}$, $Y = \max\{|y'_i|\}_{i=0}^{N-1}$, $S = \max\{|s_k|\}_{k=0}^{K-1}$, $T = \max\{|t_k|\}_{k=0}^{K-1}$ following the "centering" step, $m_{\mathrm{sp}} = 2\pi b$, $b$ is chosen by successive approximations of the equation

$$b = \frac{1}{\gamma}\log\left(\frac{4\alpha}{e}b + \frac{9\alpha}{e}\right),$$
$$\text{with } \alpha = 2 + \frac{1}{\sqrt{2\pi}},$$
$$\gamma = \pi^2\left(1 - \frac{2}{R^2}\right) \tag{7}$$

and $e$ is the requested accuracy [4].

### E. "Optimality" of the Approach

Concerning the evaluation of (2) as a matrix-vector multiplication, we refer to the linear computational model [9]. In this respect, Winograd's theorem provides an evaluation of the complexity that is $K(2N-1)$ for a "generic" rectangular $K \times N$ matrix [9]. According to Moregenstern's theorem [8], we expect that, if the computation is rearranged in terms of Fourier matrices, the complexity can be significantly reduced.

An estimate of the complexity reduction is now in order. The input sample locations [red crosses in Fig. 2 (left)] are available with the sampling step employed for their calculations, typically nonuniform, which can be in the order of, say, $\lambda/10$, as a result of the numerical solution of Maxwell equations in a scattering case. Opposite to that, the sampling steps $\Delta x$ and $\Delta y$ arising from the above-mentioned scheme to get an accuracy up to machine precision (in double-precision arithmetics) of the far-field radiation operator (Section II-B) are in the order of $\Delta x \sim \Delta y \sim \lambda/4$ according to [4]. Consequently, if we assume that the radiator/scatterer is contained within the minimum box of sides $2B \times 2B$ (see Fig. 1),[1] then $K \simeq \frac{20B}{\lambda}$ [11] and $N \simeq \left(\frac{20B}{\lambda}\right)^2 \simeq K^2$, so that $K(2N-1) \sim O(K^3)$. On the other side, the standard FFT step above costs $L^2 \log L$ with $L = \frac{8B}{\lambda} \simeq \frac{K}{2}$, whereas Steps #1 and #3 cost $O(N) = O(K^2)$ and $O(K)$, respectively. In conclusion, the matrix-vector multiplication costs $O(K^3)$, whereas the proposed approach costs $O(K^2 \log K)$ to get the FFP with machine precision.

For the purposes of Step #3, the FFT samples are required at only the blue-filled circles of Fig. 2 (right). Accordingly, a "pruned" FFT is a further possibility to save computations [5].

## III. PRUNED FFT ALGORITHM

The computational saving of pruned FFTs depends on the required output samples pattern. For 1-D FFTs of length, say $W$, when only the first few $V$ output samples are required, pruning can reduce the computational complexity from $O(W \log_2 W)$ to $O(W \log_2 V)$ [5].

In the 2-D case [12], similar results can be obtained for some specific patterns, for instance, when the output samples are organized in strips or blocks of proper size with axes parallel to the coordinate axes. Unfortunately, for the output samples pattern in Fig. 2 (right), the asymptotic computational complexity is less favorable, keeping $O(W^2 \log_2 W)$, since the output samples have a less favorable spatial organization than blocks or strips. To roughly estimate it, we use a "surface" approach. To this end, we can approximate the output pattern in Fig. 2 (right) by a circular annulus of radius $B$ (expressed in terms of power-of-two number of samples[2]) and width $\Delta B$, where $\Delta B$ is related to the spreading $2m_{\mathrm{sp}}+1$. An upper bound for the annulus surface is $2\pi B\Delta B$. This surface is proportional to the number of output, i.e., "active" butterflies of the radix $2 \times 2$ computational tree.[3] The number of overall radix $2 \times 2$ computational stages is $\log_2(2B)$, while an upper bound for the number of pruned stages can be easily calculated by assuming that, tracing back the tree, the number of "active" butterflies quadruplicates. Accordingly, the number of pruned stages $p$ can be estimated by equating $(2\pi B\Delta B)4^p = (2B)^2$, which leads to $p = 0.5\log_2(2B/(\pi\Delta B))$. Furthermore, the operations count in the unpruned case grows as $(2B)^2 \log_2(2B)$ and the order of saved operations is

$$(2B)^2\left[\frac{1}{2}\log_2\left(\frac{2B}{\pi\Delta B}\right)\right] - (2\pi B\Delta B)\sum_{k=0}^{\frac{1}{2}\log_2\left(\frac{2B}{\pi\Delta B}\right)-1} 4^k. \tag{8}$$

Therefore, an estimate of the relative computational saving is well approximated by

$$\frac{1}{2} - \frac{1}{2}\frac{\log_2(\pi\Delta B) + \frac{2}{3}}{\log_2(2B)}. \tag{9}$$

[1] We suppose that the radiator/scatterer essentially fits a square box. In the opposite case, a domain decomposition into rectangular boxes can be fruitfully exploited for an efficient hierarchical computation.

[2] More sophisticated schemes dealing with non-power-of-two number of samples can be exploited.

[3] Approaches more efficient than radix $2\times$ 2 that however do not change the asymptotic complexity are known, but are outside the scope of this estimation.

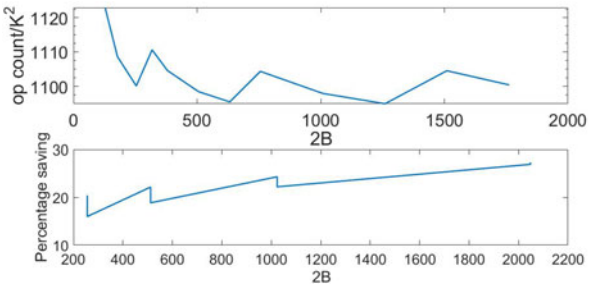


Fig. 3. Computational performance. Upper panel: number of multiplication operations normalized by $N$ against $\sqrt{N}$. Lower panel: percentage operation saving due to the use of a pruned 2-D FFT.

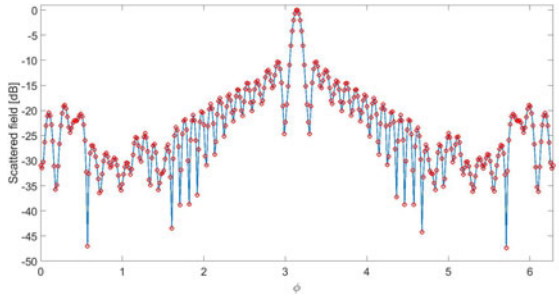


Fig. 4. FFP scattered by the homogeneous dielectric cylinder. Blue solid line: proposed approach. Red circles: exact evaluation of (2).

Consequently, a saving "logarithmically" approaching $50\%$ can be expected.

## IV. Numerical Results

The complexity and the accuracy of the proposed scheme are now assessed. For all the results, a customized version of the 2-D (pruned) radix $2 \times 2$, *decimation-in-frequency* FFT algorithm has been implemented. Memory is saved by in-place calculations. The computational burden is evaluated in terms of the number of performed multiplications, rather than giving particular focus on computation time. This is because the timing performance of actual implementations may strongly depend on software/hardware factors, such as memory latencies or exploitations of cache memories and computation pipelines, which are beyond the scope of this contribution, as in [13]. We stress that the currents considered in this section can be primary or be the contrast source in the case of scattering.

In Fig. 3, we consider the radiation by 2-D sources having circular cross section and radii $a$ comprised between 5 and $70\,\lambda$. The sources have been discretized into $N = (2\beta a)^2$ points, whereas the FFP has been calculated at $K = 2\beta a$ points. The upper panel of Fig. 3 then shows the number of multiplications required by the FFP computation divided by $K^2$. As it can be seen, the operations count grows as $K^2$ (the curve keeps practically constant), instead of $K^2 \log K$. This is due to the predominance of Step #1 for the considered sizes of the volumetric sources and to the fact that the complexity of Step #1 grows as $O(K^2)$. Such a predominance is, in turn, due to the employed (Gaussian) windows. We are already aware that other kinds of significantly more compact windows can be used, while achieving the same accuracy and drastically reducing $m_{\rm sp}$ to about 3 or 6 for single or double precision, respectively, instead of 18. Note that single precision may be already satisfactory in many applications. Work along this direction is in progress. From the bottom panel of Fig. 3, illustrating the saving due to pruning, a $25\%$ saving, coherent with (9), is observed.[4]

To assess the accuracy, we consider the scattering of a plane wave, with unit amplitude, traveling in the positive direction of the $x$-axis by a homogeneous circular cylinder of radius $a = 5\,\lambda$ and relative dielectric permittivity equal to 2.1. The cylinder has been discretized by a triangular mesh of side equal to $\lambda/8$.

[4]The "steps" in the bottom panel of Fig. 3 are due to abrupt changes of the FFT size in (5) when increasing $a/\lambda$.

The common Rao–Wilton–Glisson basis functions have been exploited to represent the contrast source current over the whole domain $S$ and proper quadrature formulas leading to (2) have been exploited [14]. Fig. 4 shows the satisfactory agreement between the FFP as evaluated by the proposed approach at the points $(\beta\cos\phi_k, \beta\sin\phi_k)$ and that computed by an exact evaluation of (2). The root mean square error between the two calculations has been $2.654 \cdot 10^{-11}$, practically approaching machine accuracy in double precision arithmetics.

For the extension to the 3-D case, a hierarchical partitioning of the computation domain in blocks chosen to reduce the burdening caused by the locations where the current samples vanish [which, for the 2-D case, have been represented by the black empty circles in Fig. 2 (left)] will be particularly useful.

## References

[1] R. Pike and P. Sabatier, Eds., *Scattering: Scattering and Inverse Scattering in Pure and Applied Science*. San Diego, CA, USA: Academic, 2002.
[2] A. Capozzoli, C. Curcio, G. D'Elia, and A. Liseno, "Fast phase-only synthesis of conformal reflectarrays," *Microw., Antennas Propag.*, vol. 4, no. 12, pp. 1989–2000, Dec. 2010.
[3] A. Boag and C. Letrou, "Fast radiation pattern evaluation for lens and reflector antennas," *IEEE Trans. Antennas Propag.*, vol. 51, no. 5, pp. 1063–1068, May 2003.
[4] A. Capozzoli, C. Curcio, A. Liseno, and A. Riccardi, "Parameter selection and accuracy in type-3 non-uniform FFTs based on Gaussian gridding," *Prog. Electromagn. Res.*, vol. 142, pp. 743–770, 2013.
[5] H. V. Sorensen and C. S. Burrus, "Efficient computation of the DFT with only a subset of input or output points," *IEEE Trans. Signal Process.*, vol. 41, no. 3, pp. 1184–1200, Mar. 1993.
[6] A. Abubakar, W. Hu, P. M. van den Berg, and T. M. Habashy, "A finite-difference contrast source inversion method," *Inverse Probl.*, vol. 24, no. 6, pp. 1–17, Sep. 2008.
[7] J. H. Richmond, "Scattering by a dielectric cylinder of arbitrary cross section shape," *IEEE Trans. Antennas Propag.*, vol. AP-13, no. 3, pp. 334–341, May 1965.
[8] J. Morgenstern, "Note on a lower bound on the linear complexity of the fast Fourier transform," *J. ACM*, vol. 20, no. 2, pp. 305–306, Apr. 1973.
[9] P. Bürgisser, M. Clausen, and M. A. Shokrollahi, *Algebraic Complexity Theory*. Berlin, Garmany: Springer-Verlag, 1997.
[10] R. M. Trigub and E. S. Belinsky, *Fourier Analysis and Approximation of Functions*. Dordrecht, The Netherlands: Springer, 2004.
[11] W. C. Chew, Y. M. Wang, G. Otto, D. Lesselier, and J. C. Bolomey, "On the inverse source method of solving inverse scattering problems," *Inverse Probl.*, vol. 10, no. 3, pp. 547–553, 1994.
[12] K.-Y. Byun, C.-S. Park, J.-Y. Sun, and S.-J. Ko, "Vector Radix $2 \times 2$ sliding fast Fourier transform," *Math. Probl. Eng.*, vol. 2016, 2016, Art. ID 2416286.
[13] M. Frigo and S. G. Johnson, "The design and implementation of FFTW3," *Proc. IEEE*, vol. 93, no. 2, pp. 216–231, Feb. 2005.
[14] S. M. Rao, D. R. Wilton, and A. W. Glisson, "Electromagnetic scattering by surfaces of arbitrary shape," *IEEE Trans. Antennas Propag.*, vol. AP-30, no. 3, pp. 409–418, May 1982.